Revision 4

A new biogenic, struvite-related phosphate, the ammonium-analogue of hazenite, $(NH_4)NaMg_2(PO_4)_2 \cdot 14H_2O$

Hexiong Yang[1], Livia Martinelli[2,3], Flavia Tasso[3], Anna Rosa Sprocati[3], Flavia Pinzari[2,4], Zhenxian Liu[5], Robert T. Downs[1], and Henry J. Sun[6]

[1]Department of Geosciences, University of Arizona, 1040 E. 4th Street, Tucson, Arizona 85721, USA
[2]Istituto Centrale per il Restauro e la Conservazione del Patrimonio Archivistico e Librario, Rome, Italy
[3]Unità Tecnica Caratterizzazione, Prevenzione e Risanamento Ambientale, ENEA-CASACCIA, Rome, Via Anguillarese 301, 00123 Rome, Italy
[4]Consiglio per la Ricerca e la sperimentazione in Agricoltura Centro di ricerca per lo studio delle relazioni tra pianta e suolo. Via della Navicella 2-4, 00184 Rome, Italy
[5]Geophysical Laboratory, Carnegie Institution of Washington, Washington, D.C. 20015, USA
[6]Desert Research Institute, 755 Flamingo Road, Las Vegas, Nevada 89119, USA

Abstract

A new biogenic, struvite-related phosphate, the ammonium analogue of hazenite (AAH), ideally $(NH_4)NaMg_2(PO_4)_2 \cdot 14H_2O$, has been found in cultures containing the bacterial strain *Virgibacillus* sp.NOT1 (GenBank Accession Number: JX417495.1) isolated from an XVII Century document made of parchment. The chemical composition of AAH, determined from the combination of electron microprobe and X-ray structural analyses, is $[(NH_4)_{0.78}K_{0.22}]NaMg_2(PO_4)_2 \cdot 14H_2O$. Single-crystal X-ray diffraction shows that AAH is orthorhombic with space group *Pmnb* and unit-cell parameters a = 6.9661(6), b = 25.236(3), c = 11.292(1) Å, and V =1985.0(3) Å^3. Compared to hazenite, the substitution of NH_4^+ for K^+ results in a noticeable increase of the average A-O (A = $NH_4^+ + K^+$) bond length and the unit-cell volume for AAH, as also observed for struvite vs. struvite-K. Both infrared and Raman spectra of AAH resemble those of hazenite, as well as struvite. Our study reveals that AAH forms only in cultures with Na-bearing solutions and pH below 10.0. No AAH or hazenite was found in experiments with

the K-bearing solutions, suggesting the necessity of a Na-bearing solution for AAH formation.

***Key words*:** ammonium phosphate, hazenite, struvite-type materials, biomineral, crystal structure, X-ray diffraction, infrared and Raman spectra

Introduction

Phosphate formation through microbial activities is one of the most common mechanisms for the biological transformation of inorganic phosphates (Gibson 1974; Kamnev et al. 1999; Desmidt et al. 2013). Among all biogenic phosphates, struvite, $(NH_4)MgPO_4 \cdot 6H_2O$, is the most widespread in a variety of environments, such as bat droppings, decomposing foods, infection (e.g., urinary tract) stones in humans, water treatment facilities, and in a range of bacterial cultures (Sánchez-Román et al., 2007; Weil 2008; Desmidt et al. 2013 and references therein). The specific roles that microorganisms play in struvite formation are not well understood. It has been speculated that bacterial cell surfaces may serve as nucleation sites and biological activities provide a steady supply of phosphate and ammonia as the crystals grow (e.g., Ben Omar 1994, 1995, 1998; Chen et al. 2010).

A number of compounds are isotypic with, or structurally analogous to, struvite (Dickens and Brown 1976; Weil 2008; Yang et al. 2011). A general chemical formula for struvite-type materials can be expressed as $A^+M^{2+}(XO_4)\cdot nH_2O$, where n = 6 - 8, X = P or As, A = NH_4, K, Rb, Cs, and Tl, and M = Mg, Fe, Co, Ni, Zn, Mn. A common structural feature of struvite-type compounds is that all M cations are octahedrally coordinated by six H_2O molecules and no H_2O molecule is shared between $M(H_2O)_6$ octahedra. The XO_4 tetrahedra and $M(H_2O)_6$ octahedra are interlinked through hydrogen bonding. The struvite-type structure was once thought unable to accommodate A cations smaller than K^+ (Banks et al. 1975). Nevertheless, Mathew et al. (1982) synthesized a Na-analogue of struvite, $NaMg(PO_4)\cdot 7H_2O$, in which the small Na^+ (relative to K^+) is compensated by an

59 additional H_2O molecule. More intriguingly, Yang and Sun (2004) and Yang et al. (2011)
60 described the new biomineral hazenite, $KNaMg_2(PO_4)_2 \cdot 14H_2O$, which possesses many
61 structural features similar to those for both struvite-(K), $KMg(PO_4) \cdot 6H_2O$ (Mathew and
62 Schroeder 1979; Graeser et al. 2008) and synthetic $NaMg(PO_4) \cdot 7H_2O$ (Mathew et al.
63 1982). Hazenite represents the first struvite-type phosphate that contains both K and Na
64 as the *A* ions. In this paper, we report a new biologically-formed phosphate, an
65 ammonium analogue of hazenite, ideally $(NH_4)NaMg_2(PO_4)_2 \cdot 14H_2O$.
66
67 **Experimental Methods**
68 **Formation of the ammonium analogue of hazenite (AAH)**
69 The AAH crystals used in this study were formed in cultures containing the
70 bacterial strain *Virgibacillus* sp.NOT1 (GenBank Accession Number: JX417495.1),
71 which was isolated from an XVII Century document made of parchment and identified
72 through 16S rDNA sequencing. The growth medium was prepared in Blood Agar Base
73 N.2 (Oxoid, Code: CM0271) with the following components: Proteose peptone 15.0 g/L;
74 liver digest 2.5 g/L; yeast extract 5.0 g/L; sodium chloride 5.0 g/L, agar 12.0 g/L. The
75 final pH was 7.4(2) at 25°C. Four different salts at two or three different concentrations
76 were added to the growth media (Table 1). A 10-ml aliquot of each salt-supplemented
77 agar medium was used for the pH measurements before solidification using a glass
78 electrode specific for high viscosity samples (Metrhom 6.0239.100 Viscotrode). The
79 plates were then inoculated by surface streaking and incubated aerobically at 25 °C.
80 Cultures were checked for crystal formation periodically for up to 60 days. As the growth
81 media began to dry, elongated tabular or prismatic AAH crystals (up to $0.50 \times 0.12 \times$
82 0.08 mm) appeared on or in the bacterial colonies in runs #1, 2, and 4 (Fig. 1).
83
84 **Characterization of AAH crystals**

The AAH crystals were first examined using a Variable Pressure EVO 50 Scanning Electron Microscope. Qualitative chemical analysis of AAH was performed with electron-dispersive spectroscopy following the procedure given by Gazulla et al. (2013), which revealed the major elements P, Mg, Na, K, and N, plus trace Ca. The presence of N in AAH was further confirmed by the infrared (IR) spectroscopy and X-ray structure determination (see below).

The quantitative analysis of the AAH chemical composition was conducted with a CAMECA SX100 electron microprobe at 10 kV and 5 nA, with a beam size of 20 μm to minimize the sample damage by the electron beam. The average composition of five analysis points is (wt.%): P_2O_5 42.2(4), MgO 23.7(3), Na_2O 9.0(1), K_2O 2.5(2), and CaO 0.16(8), with a sum of 77.5(6) wt.%. Due to the high degree of hydration and the rapid deterioration of the sample during the microprobe analysis, this composition was used only for the estimation of cation ratios. By assuming two P cations per formula, the relative ratio of P:Mg:Na:K is 2.00:1.98:0.98:0.18. The actual composition of the crystal, $[(NH_4)_{0.78}K_{0.22}]NaMg_2(PO_4)_2 \cdot 14H_2O$, was determined by the combination of the electron microprobe and X-ray structural analyses (see below), which can be idealized as $(NH_4)NaMg_2(PO_4)_2 \cdot 14H_2O$.

The IR and Raman spectra of AAH were acquired at the U2A beam line of the National Synchrotron Light Source at Brookhaven National Laboratory. The details of experimental procedures and the optical layout of the beamline have been described by Liu et al. (2002).

Single-crystal X-ray diffraction data of AAH (from run 2) were collected at ambient temperature on a Bruker X8 APEX2 CCD X-ray diffractometer equipped with graphite-monochromatized MoK_α radiation. All reflections were indexed on the basis of an orthorhombic unit-cell (Table 2). The intensity data were corrected for X-ray absorption using the Bruker program SADABS. The systematic absences of reflections suggest possible space group *Pmnb* (#62) or $P2_1nb$ (#33). The structure model of hazenite

(Yang et al. 2011) was adopted and refined using SHELX97 (Sheldrick 2008) based on the space group *Pmnb*, because it yielded the better refinement statistics in terms of bond lengths and angles, atomic displacement parameters, and *R* factors. The H atoms in all H_2O molecules were located, but not those in NH_4^+. The positions of all atoms were refined with anisotropic displacement parameters, except for H atoms, which were refined with a fixed isotropic displacement parameter (U_{eq} = 0.04). The site occupancy of K was refined against N, yielding a relative ratio of 0.22(1) : 0.78(1). This ratio was adopted in our empirical formula for AAH. Final coordinates and displacement parameters of atoms are listed in Table 3, and selected bond-distances in Table 4.

Discussion

Crystal Structure

AAH is isostructural with hazenite, which exhibits many structural features resembling those of struvite-type materials (Yang and Sun 2004; Yang et al. 2011). The crystal structure of AAH is characterized by six distinct non-hydrogen cation sites, including two octahedral sites for Mg^{2+} (Mg1 and Mg2), two tetrahedral sites for P^{5+} (P1 and P2), one trigonal prismatic site for Na^+, and one six-coordinated, very irregular site for A^+. These cation sites form three types of layers that are stacked along the *b*-axis in a repeating sequence of ABCBABCB… (Fig. 2), where layer A consists of $Mg1(H_2O)_6$ octahedra and NaO_6 trigonal prisms, layer B of $P1O_4$ and $P2O_4$ tetrahedra, and layer C of $Mg2(H_2O)_6$ octahedra and AO_6 polyhedra. These layers are linked together by hydrogen bonds, plus the *A*-O bonds between layers B and C (*A*-O5-P2). As noted by Yang et al. (2011), the struvite-type structure, which displays a layer stacking sequence of BCBCBC..., can be readily derived from the hazenite-type structure by replacing its layer A with layer C.

In general, because the effective radius of NH_4^+ (1.48 Å) is larger than that of K^+ (1.38 Å for six-coordination) (Shannon 1976), the substitution of NH_4^+ for K^+ in a crystal

will result in the increase in both the average *A*-O bond length and the unit-cell volume, as have been observed in numerous compounds (e.g. Abu El-Fadl et al. 2006; Bogdanov et al. 2011; Shin 2011; Lim and Lee 2013). For AAH and hazenite, the average *A*-O bond lengths are 2.972 and 2.919 Å (Yang et al. 2011), respectively (Table 4), and the unit-cell volumes are 1985.0(5) and 1958.7(2) $Å^3$ (Table 5). Similar results are also found for struvite vs. struvite-K (Table 5).

Infrared and Raman spectra

Figures 3 and 4 show the IR and Raman spectra of AAH. There have been copious IR and Raman spectroscopic studies on struvite-related materials (Banks et al. 1975; Angoni et al. 1998; Stefov et al. 2004, 2005; Frost et al. 2005; Koleva 2007; Cahil et al. 2008). Yang and Sun (2004) and Yang et al. (2011) showed that the IR and Raman spectra of hazenite are similar to those of struvite and made the tentative assignments of major bands for both spectra. These assignments should be applicable to AAH as well because of their isotypism. Nonetheless, as in the case for struvite vs. struvite-K (e.g., Stefov et al. 2005; Cahil et al. 2008), the IR spectrum of AAH is expected to be more complicated than that of hazenite owing to the presence of the significant amount of NH_4^+. The presence of NH_4^+ in crystals generally gives rise to two discernible groups of bands: one at ~1430 cm^{-1} attributable to the H-N-H bending vibrations and the other at ~3300 cm^{-1} originating from the N-H stretching vibrations, although the exact numbers and positions of bands in each group may vary, depending on the bonding environments and the local symmetry of NH_4^+. For AAH, the bands ascribable to the H-N-H bending vibrations are observed at ~1379 and 1388 cm^{-1}. However, it is difficult to unambiguously assign which bands arise from the N-H stretching vibrations due to overlap with the O-H stretching vibrations in the range of 2700 to 3700 cm^{-1}.

Compared to the band positions for the H-N-H bending vibrations for AAH, those for struvite are at much greater wavenumbers (~1432 and 1468 cm^{-1}) (Figure 3). This

166 evident difference is related to the bonding environments around NH_4^+ in the two
167 compounds. In struvite, NH_4^+ is coordinated by six O atoms, with a wide range of the N-
168 O distances, from 2.800 to 3.498 Å, and an average N-O distance of 3.136 Å (Ferraris et
169 al. 1986), whereas all six O atoms coordinated to *A* in AAH fall between 2.720 and 3.095
170 Å, with an average *A*-O distance of 2.972 Å (Table 4) [see Yang and Sun (2004) for a
171 detailed discussion on the bonding differences around the *A* site between the hazenite-
172 and struvite-type structures]. While the large separation between the two H-N-H bending
173 modes (1468 – 1432 = 36 cm^{-1}) for struvite is primarily a consequence of the marked
174 distortion of its A site, the greater wavenumbers of the two bending bands in struvite
175 (relative to those in AAH) may be explained by its longer average N-O distance. For a N-
176 H…O bond, the longer N-O distance means a stronger N-H and weaker H…O bonding,
177 which makes the H-N-H bending more difficult and the corresponding bands appear at
178 higher wavenumbers.
179
180 **Implications of AAH**
181 As shown in Table 1, AAH appears to form only in cultures with the Na-bearing
182 solutions and pH below 10.0 (runs #1, 2, and 4). No AAH or hazenite was found in
183 experiments with the K-bearing solutions (runs 7-10). Hence, a Na-rich environment
184 seems to be essential for the formation of both AAH and hazenite (Yang and Sun 2004).
185 In addition, we observed both AAH and struvite in run #1, suggesting that they are
186 overlapping in formation environments. In nature, Mono Lake in California, which is
187 known for its unique biological and geochemical features, currently consists of a
188 hypersaline (84–92 g/L), alkaline (pH = 9.8) Na-CO_3-Cl-SO_4 brine (Yang et al. 2011 and
189 references therein). This environment is obviously analogous to that of our experimental
190 run #1 or #2. Hazenite was discovered on the south shore of Mono Lake (Yang et al.
191 2011), where no struvite has been documented. However, on the north shore of the lake,
192 especially on Paoha Island, where guano is relatively well preserved, struvite is quite

193 abundant (Cooper and Dunning 1969; Walker 1988). These places, therefore, could serve
194 as candidates for the formation and discovery of AAH in nature.

195 Research on the precipitation of struvite from sewage has been an attractive
196 subject as it may offer a potential route for dephosphorization of wastewater from
197 industries and recovery of phosphates for fertilizers (e.g., Doyle and Parsons 2002; Shu et
198 al. 2006; Forrest et al. 2008; Machnicha et al. 2008; Muster et al. 2013). Given the strong
199 resemblances in both chemistry and structure between struvite and AAH, a better
200 understanding of the formation mechanism of AAH, especially in terms of the extent of
201 bacterial involvements, will unquestionably provide additional knowledge of
202 biomineralization of struvite-type phosphate materials and might lead to another route
203 for dephosphorization of wastewater. Furthermore, the struvite-type structure allows a
204 complete substitution of AsO_4^{3+} for PO_4^{3+} (Weil 2008 and references therein). Thus, it
205 would be intriguing to explore whether the hazenite-type structure can also have the As-
206 analogues, synthetic or natural.
207

208 **Acknowledgements**

209 This study was supported by the Science Foundation Arizona. The authors are
210 grateful to Piero Colaizzi from the Istituto Centrale per il Restauro e la Conservazione del
211 Patrimonio Archivistico e Librario of Rome for his kind technical assistance with SEM-
212 EDS. The careful and constructive reviews by Drs. W. Kolitsch and J. Pasteris are greatly
213 appreciated.
214
215

216 **References Cited**

217 Abu El-Fadl, A., Soltan, A.S., and Shaalan, N.M. (2006) Influence of cationic

substitution on lattice constants and optical characterization in solution grown mixed crystals of potassium-ammonium zinc chloride. Crystal Research and Technology, 41, 1013-1019.

Angoni, K., Popp, J., and Kiefe, W. (1998) A vibrational spectroscopy study of “urinary Sand”. Spectroscopy Letters, 31, 1771-1782.

Abbona, F., Calleri, M., and Ivaldi, G. (1984) Synthetic struvite, $MgNH_4PO_4 \cdot 6H_2O$: Correct polarity and surface features of some complementary forms, Acta Crystallographica, B40, 223-227.

Banks, E., Chianelli, R., and Korenstein, R. (1975) Crystal chemistry of struvite analogs of the type $MgMPO_4 \cdot 6H_2O$ ($M^+ = K^+$, Rb^+, Cs^+, Tl^+, NH_4^+). Inorganic Chemistry, 14, 1634-1639.

Ben Omar, N., Entrena, M., Gonzalez-Munoz, M.T., Arias, J.M., and Huetas, F. (1994) The effects of pH and phosphate on the production of struvite by *Myxococcus Xanthus*. Geomicrobiology Journal, 12, 81-90.

Ben Omar, N., Matinez-Canamero, M., Gonzalez-Munoz, M.T., Arias, J.M., and Huetas, F. (1995) *Myxocuccus* xanthus’ killed cells as inducers of struvite crystallization: Its possible role in the biomineralization processes. Chemosphere, 30, 2387-2396.

Ben Omar, N., Gonzalez-Munoz, M.T., Penalver, J.M.A. (1998) Struvite crystallization on *Myxocuccus* cells. Chemosphere, 36, 475-481.

Bogdanov, E.V., Vasil’ev, A.D., Flerov, I.N., and Laptash, N.M. (2011) Effects of cation substitution in fluorine-oxygen molybdates $(NH_4)_{2-x}A_xMoO_2F_4$. Physics of the Solid State, 53, 303-308.

Cahil, A, Soptrajanov, B., Najdoski, M, Lutz, H.D., Engelen, B., and Stefov, V. (2008) Infrared and Raman spectra of magnesium ammonium phosphate hexahydrate (struvite) and its isomorphous analogues. Part VI: FT-IR spectra of isomorphous isolated species. NH_4^+ ions isolated in $MKPO_4 \cdot 6H_2O$ (M = Mg, Ni) and PO_4^{3-}

ions isolated in $MgNH_4AsO_4 \cdot 6H_2O$. Journal of Molecular Structure, 876, 255-259.

Chen, L., Shen, Y., Xie, A., Huang, F., Zhang, W., and Liu, S. (2010) Seed-mediated synthesis of unusual struvite hierarchical superstructures using bacterium. Crystal Growth & Design, 10, 2073-2082.

Cooper, J.F. and Dunning, G.E. (1969) Struvite found at Mono Lake. Mineral Information Service, 22, 44-45.

Desmidt, E., Ghyselbrecht, K., Monballiu, A., Rabaey, K., Verstraete, W., and Meesschaert, B. D. (2013) Factors influencing urease driven struvite precipitation. Separation and Purification Technology, 110, 150-157.

Dickens, B. and Brown, W.E. (1972) The crystal structure of $CaKAsO_4 \cdot 8H_2O$. Acta Crystallographica, B28, 3056-3065.

Doyle, J.D. and Parsons, S.A. (2002) Struvite formation, control, and recovery. Water Research, 36, 3925-3940.

Ferraris, G., Fuess, H., and Joswig, W. (1986) Neutron diffraction study of $Mg(NH_4)(PO_4).6H_2O$ (struvite) and survey of water molecules donating short hydrogen bonds. Acta Crystallographica B, 42, 253-258.

Forrest, A.L., Fattah, K.P., Mavinic, D.S. and Koch, F.A. (2008) Optimizing struvite production for phosphate recovery in WWTP. Journal of Environmental Engineering, 134, 395-402.

Frost, R.L., Weier, M.L., Martens, W.N., Henry, D.A., and Mills, S.J. (2005) Raman spectroscopy of newberyite, hannayite, and struvite. Spectroschimica Acta, A62, 181-188.

Gazulla, M.F., Rodrigo, M., Blasco, E., and Orduna, M. (2013) Nitrogen determination by SEM-EDS and elemental analysis. X-ray Spectrometry, 42 (in press. DOI 10.1002/xrs.2490).

Gibson, R.I. (1974) Descriptive human pathological mineralogy. American Mineralogist,

59, 1177-1182.

Graeser, S., Postl, W., Bojar, H.-P., Berlepsch, P., Armbruster, T., Raber, T., Ettinger, K., Walter, F. (2008): Struvite-(K), $KMgPO_4 \cdot 6H_2O$, the potassium equivalent of struvite – a new mineral. European Journal of Mineralogy, 20, 629-633.

Kamnev, A.A., Antonyuk, L.P., Colina, M., Chernyshev, A.V., Ignatov, V. (1999) Investigation of a microbially produced structural modification of magnesium-ammonium orthophosphate. Monatshefte für Chemie, 130, 1431-1442.

Koleva, V.G. (2007) Vibrational behavior of the phosphates ions in dittmarite-type compounds M'M''PO4·H_2O (M'=K^+, NH_4^+; M''=Mn^{2+}, Co^{2+}, Ni^{2+}). Spectrochimica Acta, A66, 413-418.

Lim, A.R. and Lee, M. (2013) Structural properties in mixed $LiK_{1-x}(NH_4)_xSO_4$ (x = 0, 0.06, and 1) crystals by nuclear magnetic resonance. Journal of Molecular Structure, 1033, 113-120.

Liu, Z., Hu, J., Mao, H.K., and Hemley, R.J. (2002) High-pressure synchrotron x-ray diffraction and infrared microspectroscopy: applications to dense hydrous phases. Journal of Physics: Condensed Matter, 14, 10641–10646.

Machnicha, A., Grubel, K., and Suschka, J. (2008) Enhanced biological phosphorus removal and recovery. Water Environment Research, 80, 617-623.

Mathew, M., and Schroeder, L.W. (1979) Crystal structure of a struvite analogue, $MgKPO_4 \cdot 6H_2O$. Acta Crystallographica, B35, 11-13.

Mathew, M., Kingsbury, P., Takagi, S., and Brown, W.E. (1982) A new struvite-type compound, magnesium sodium phosphate heptahydrate. Acta Crystallographica, B38, 40-44.

Muster, T.H., Douglas, G.B., Sherman, N., Seeber, A., Wright, N., and Guezuekara, Y. (2013) Towards effective phosphorus recycling from wastewater: Quantity and quality. Chemosphere, 91, 676-684.

Sánchez-Román, M., Rivadeneyra, M.A., Vasconcelos, C., and McKenzie, J.A. (2007) Biomineralization of carbonate and phosphate by moderately halophilic bacteria. FEMS Microbiology Ecology, 61, 273-84.

Shannon, R.D. (1976) Revised effective ionic radii and systematic studies of interatomic

distances in halides and chalcogenides. Acta Crystallographica, A32, 751–767.

Sheldrick, G. M. (2008) A short history of *SHELX*. Acta Crystallographica, A64, 112-122.

Shin, H.K. (2011) Protonic conductivity and phase transition in $K_{1-x}(NH_4)_xHSO_4$. Solid State Ionics, 189, 29-32.

Shu, L., Schneider, P., Jegatheesan, V., and Johnsom, J. (2006) An economic evaluation of phosphorous recovery as struvite from digester supernatant. Bioresource Technology, 97, 2211-2216.

Stefov, V., Soptrajanov, B., Spirovski, F., Kuzmanovski, I., Lutz, H.D., and Engelen, B. (2004) Infrared and Raman spectra of magnesium ammonium phosphate hexahydrite (struvite) and its isomorphous analogues. I. Spectra of protiated and partially deuterated magnesium potassium phosphate hexahydrite. Journal of Molecular Structure, 689, 1-10.

Stefov, V., Soptrajanov, B., Kuzmanovski, I., Lutz, H.D., and Engelen, B. (2005) Infrared and Raman spectra of magnesium ammonium phosphate hexahydrite (struvite) and its isomorphous analogues. III. Spectra of protiated and partially deuterated magnesium ammonium phosphate hexahydrite. Journal of Molecular Structure, 752, 60-67.

Walker, J. (1988) Paoha Island phosphates. Quarterly of San Bernardino County Museum Association, 35, 46-47.

Weil, M. (2008) The struvite-type compounds $M[Mg(H_2O)_6](XO_4)$, where M = Rb, Tl and X = P, As. Crystal Research and Technology, 43, 1286-1291.

Yang, H. and Sun, H.J. (2004) Crystal structure of a new phosphate compound, $Mg_2KNa(PO_4)_2{\cdot}14H_2O$. Journal of Solid State Chemistry, 177, 2991-2997.

Yang, H., Sun, H. J., and Downs, R.T. (2011) Hazenite, $KNaMg_2(PO_4)_2{\cdot}14H_2O$, a new biologically related phosphate mineral, from Mono Lake, California, U.S.A. American Mineralogist, 96, 675-681.

List of Tables

List of Figure Captions

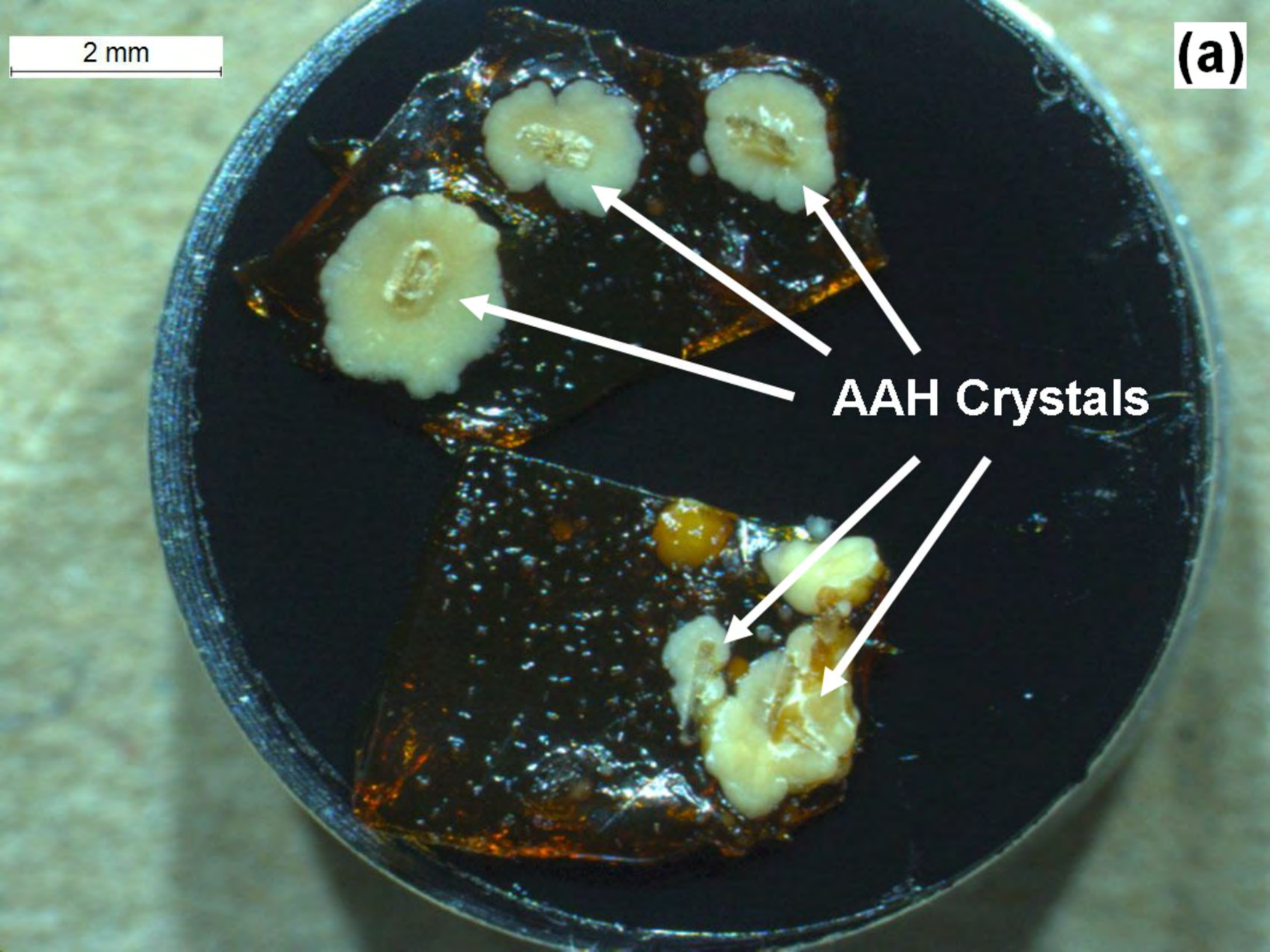
2 mm
(a)
AAH Crystals

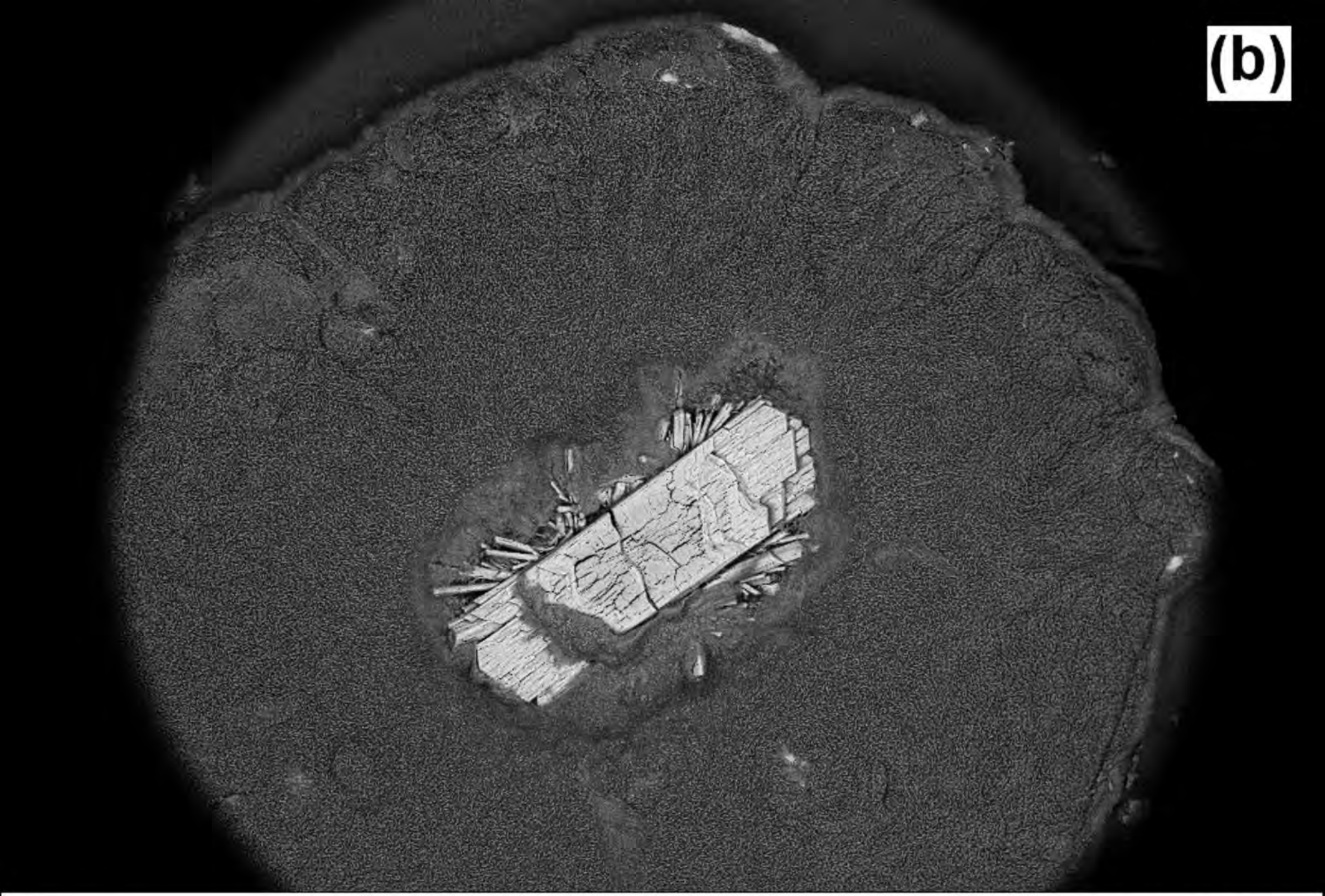
(b)
200 µm*
Mag = 152 X
File Name = Na2CO3 5% new 36.tif
Chamber = 31 Pa
Signal A = CZ BSD
Brightness = 35.0 %
Contrast = 78.0 %
I Probe = 253 pA
Spot Size = 442
EHT = 20.00 kV
WD = 12.5 mm

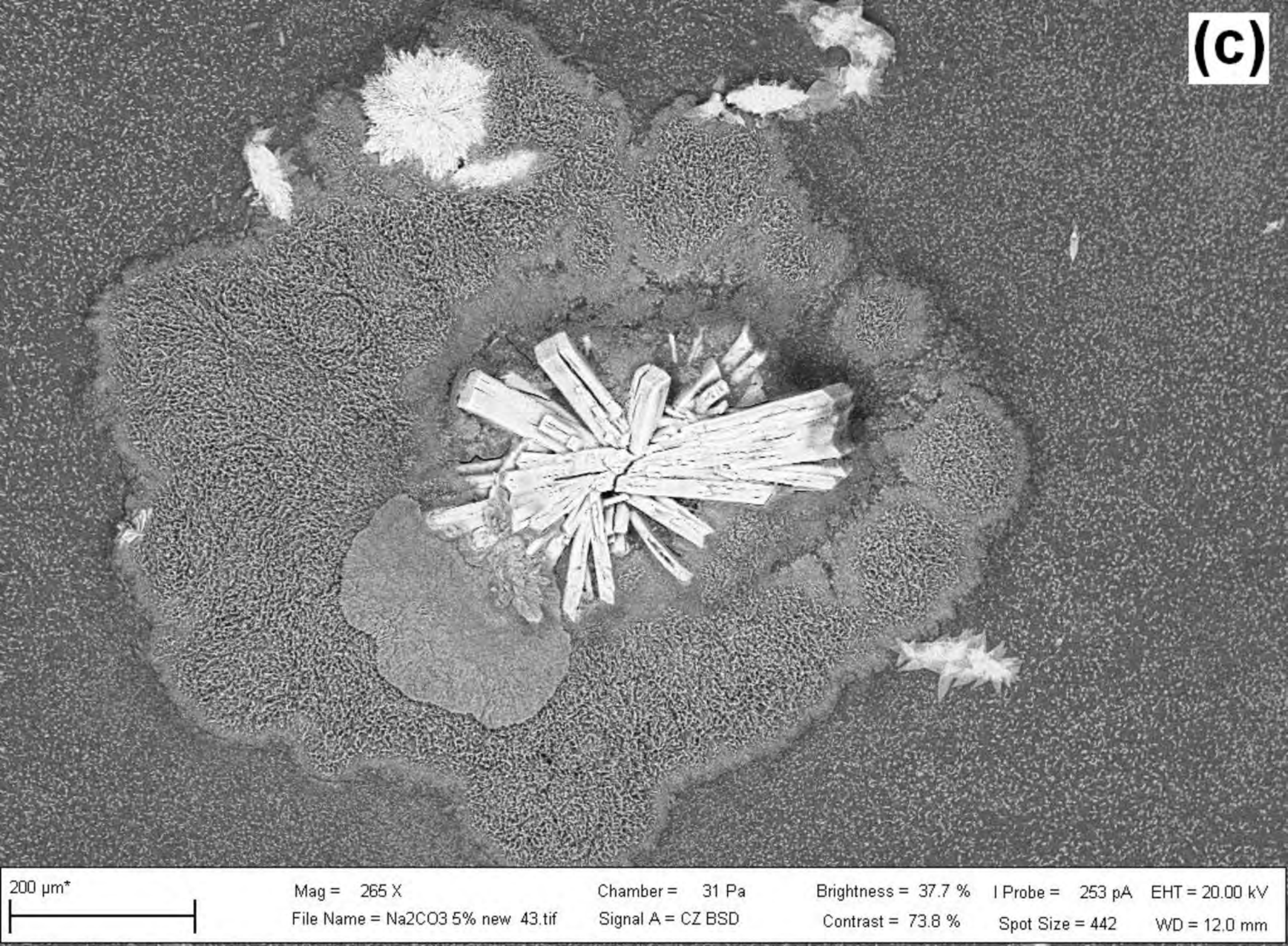
(c)
200 µm*
Mag = 265 X
File Name = Na2CO3 5% new 43.tif
Chamber = 31 Pa
Signal A = CZ BSD
Brightness = 37.7 %
Contrast = 73.8 %
I Probe = 253 pA
Spot Size = 442
EHT = 20.00 kV
WD = 12.0 mm


(d)
100 µm*
Mag = 147 X
File Name = Na2CO3 5% new 39.tif
Chamber = 31 Pa
Signal A = CZ BSD
Brightness = 33.6 %
Contrast = 78.3 %
I Probe = 253 pA
Spot Size = 442
EHT = 20.00 kV
WD = 12.5 mm

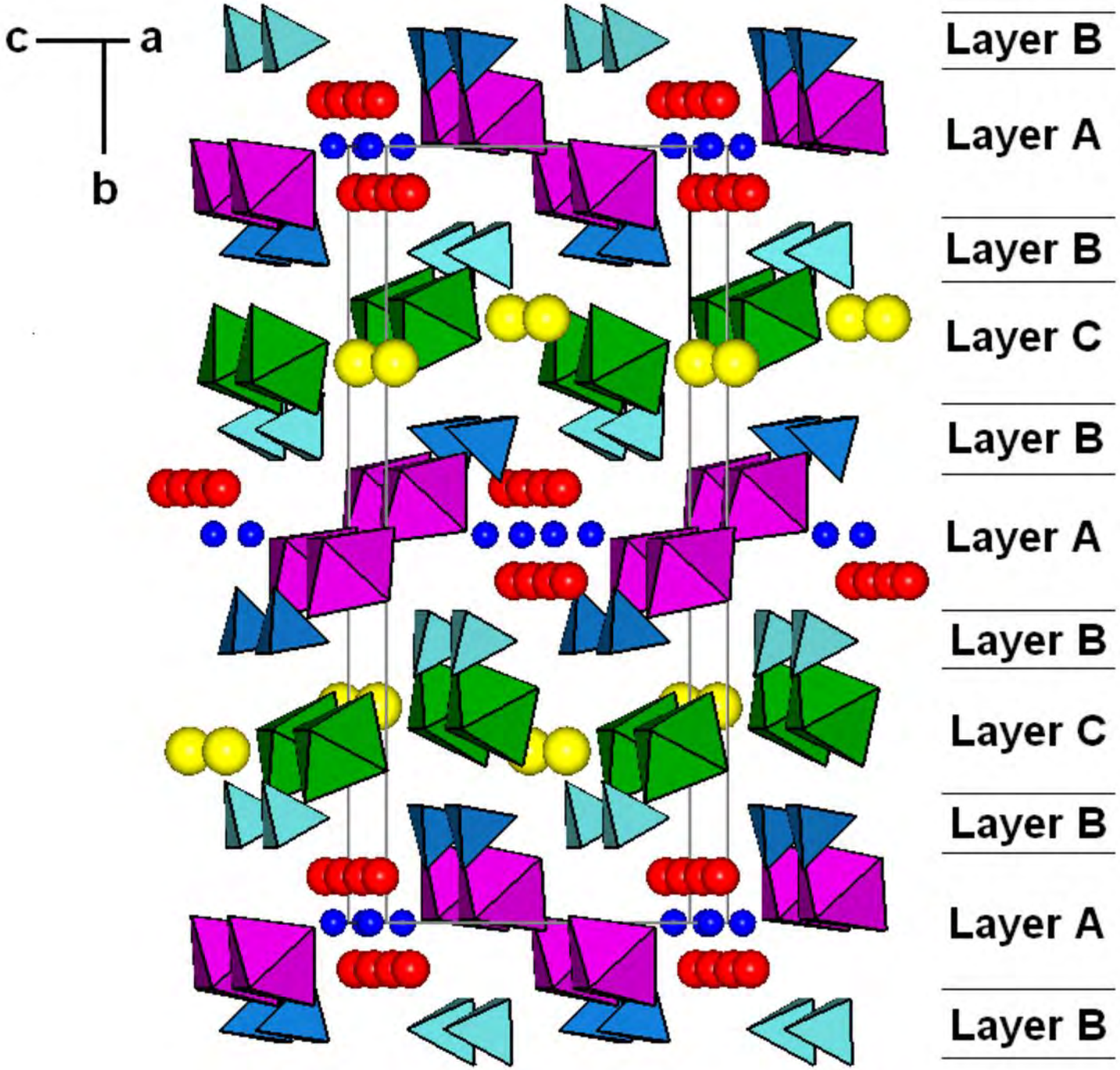
c
a
b
Layer B
Layer A
Layer B
Layer C
Layer B
Layer A
Layer B
Layer C
Layer B
Layer A
Layer B

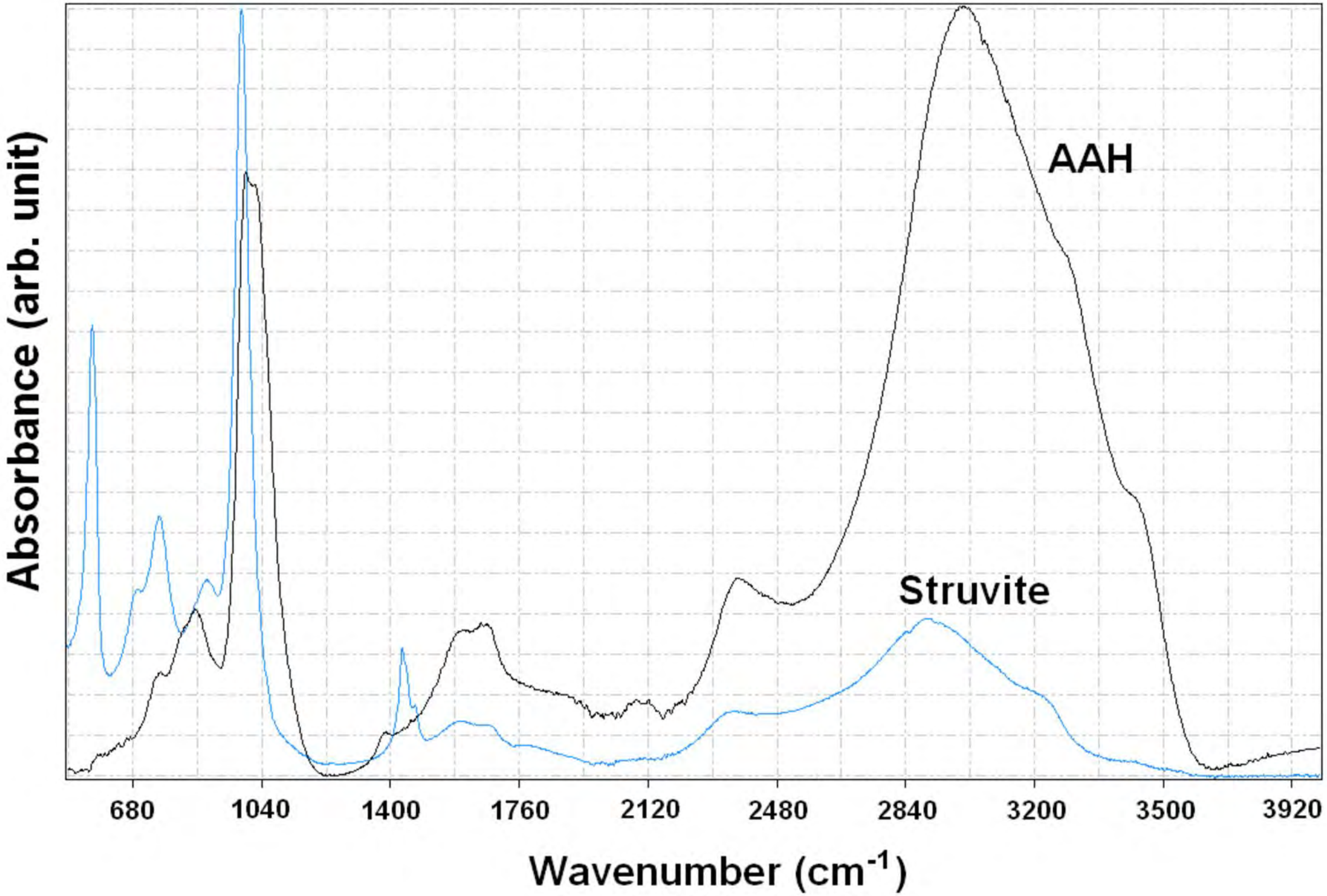
AAH
Struvite
Absorbance (arb. unit)
680
1040
1400
1760
2120
2480
2840
3200
3500
3920
Wavenumber (cm-1)

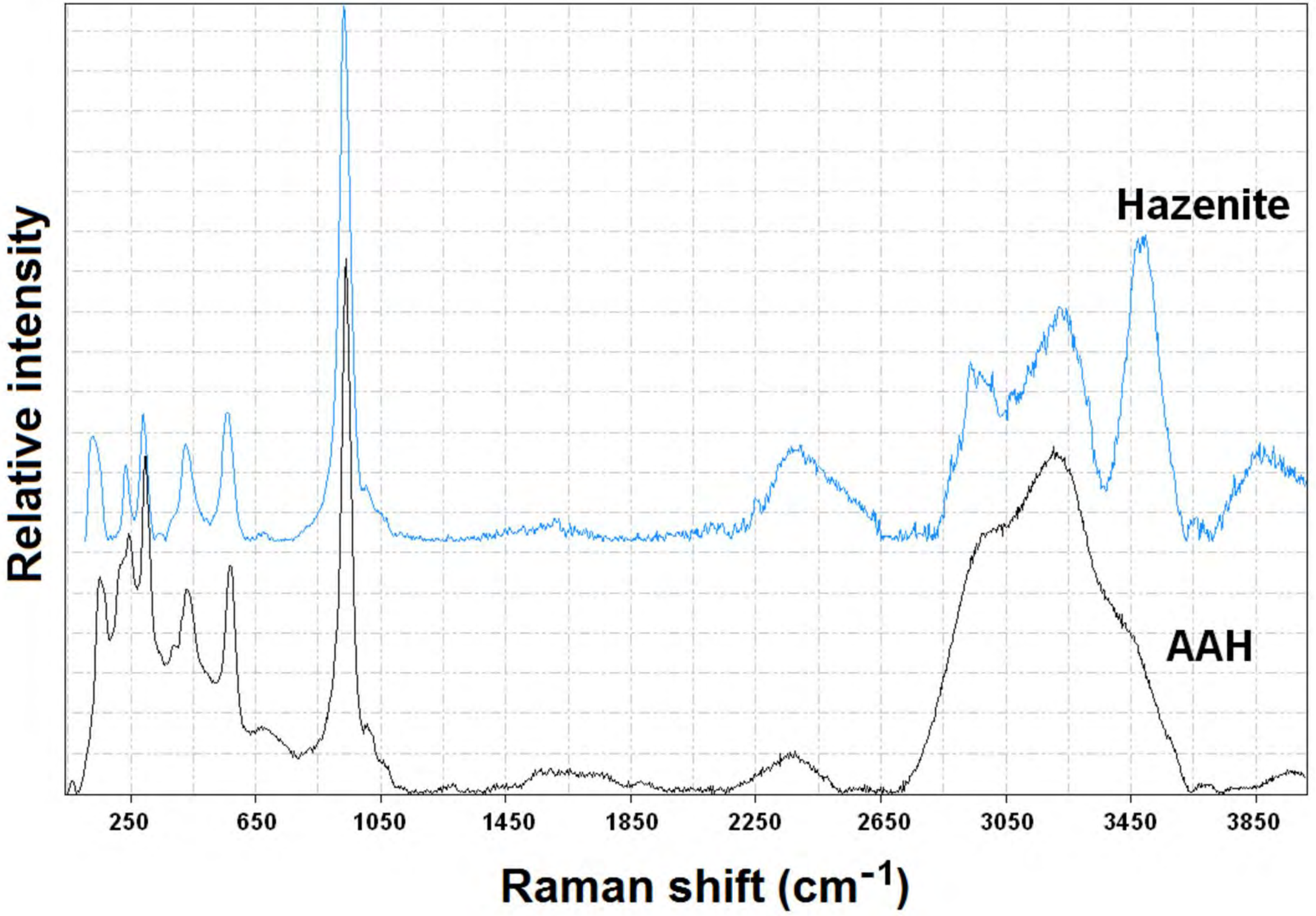
Hazenite
AAH
Relative intensity
250
650
1050
1450
1850
2250
2650
3050
3450
3850
Raman shift (cm-1)

Table 1. Agar media prepared for the biomineralization experiments.

Run #	Supplemented salt	Concentration	Final agar pH at 25°C	Products identified
1	Na_2CO_3	2%	9.5(3)	ammonium hazenite, struvite
2	Na_2CO_3	5%	9.9(2)	ammonium hazenite
3	Na_2CO_3	10%	10.0(2)	No visible crystals
4	NaCl	2%	6.9(1)	ammonium hazenite (very few)
5	NaCl	5%	6.9(4)	halite
6	NaCl	10%	6.7(3)	halite
7	KCl	5%	7.0(2)	sylvite
8	KCl	15%	6.6(1)	sylvite
9	K_2CO_3	5%	9.9(5)	struvite-K
10	K_2CO_3	15%	10.5(6)	kalincinite

*: The pH value for each run is an average of five measurements.

Table 2. Summary of crystallographic data and refinement results for ammonium analogue of hazenite

Ideal structural formula	$(NH_4)NaMg_2(PO_4)_2 \cdot 14H_2O$
Space group	*Pmnb* (No. 62)
a (Å)	6.9661(6)
b (Å)	25.236(3)
c (Å)	11.2919(11)
V (Å^3)	1985.0(3)
Z	4
ρ_{calc} (g/cm^3)	1.795
λ (Å)	0.71069
μ (mm^{-1})	0.445
θ range for data collection	1.56 to 28.28
No. of reflections collected	21864
No. of independent reflections	2646
No. of reflections with $I > 2\sigma(I)$	1962
No. of parameters refined	198
R(int)	0.068
Final R factors [$I > 2\sigma(I)$]	$R_1 = 0.042$, $wR_2 = 0.091$
Final R factors (all data)	$R_1 = 0.066$, $wR_2 = 0.099$
Goodness-of-fit	1.09

Table 3. Coordinates and displacement parameters of atoms for ammonium analogue of hazenite

Atom	x	y	z	Uiso	U11	U22	U33	U23	U13	U12
A	¾	0.22146(6)	0.4983(1)	0.0386(6)	0.0505(11)	0.0295(9)	0.0356(10)	-0.0080(6)	0	0
Na	¾	0.00057(7)	0.9266(2)	0.0367(6)	0.0280(10)	0.0420(11)	0.0401(11)	0.0115(8)	0	0
Mg1	¾	0.95466(4)	0.6394(1)	0.0143(4)	0.0139(6)	0.0142(6)	0.0149(6)	0.0021(4)	0	0
Mg2	¾	0.22385(4)	0.8370(1)	0.0160(4)	0.0185(6)	0.0152(6)	0.0141(6)	0.0007(4)	0	0
P1	¼	0.12865(3)	0.7211(1)	0.0149(2)	0.0157(4)	0.0152(4)	0.0139(4)	-0.0009(3)	0	0
P2	¾	0.12589(3)	0.2172(1)	0.0142(2)	0.0132(4)	0.0147(4)	0.0145(4)	0.0023(3)	0	0
O1	¼	0.13574(10)	0.8572(2)	0.0215(5)	0.0230(12)	0.0289(13)	0.0127(12)	-0.0019(10)	0	0
O2	¼	0.18372(9)	0.6614(2)	0.0222(5)	0.0269(13)	0.0179(11)	0.0218(12)	0.0019(10)	0	0
O3	0.4317(2)	0.09817(6)	0.6845(1)	0.0201(4)	0.0172(8)	0.0206(8)	0.0224(9)	-0.0029(6)	0.0002(7)	0.0024(7)
O4	¾	0.06616(9)	0.1907(2)	0.0241(6)	0.0229(13)	0.0153(12)	0.0341(14)	-0.0001(10)	0	0
O5	¾	0.13598(10)	0.3515(2)	0.0219(5)	0.0224(12)	0.0281(13)	0.0151(12)	0.0007(10)	0	0
O6	0.9311(2)	0.15090(6)	0.1616(1)	0.0192(4)	0.0162(8)	0.0216(8)	0.0198(8)	0.0063(7)	0.0019(7)	-0.0014(7)
OW7	¾	0.00987(12)	0.5072(3)	0.0292(7)	0.0207(14)	0.0318(16)	0.0352(16)	0.0180(12)	0	0
OW8	¾	0.89480(13)	0.7615(3)	0.0366(8)	0.0145(13)	0.0469(18)	0.0484(19)	0.0336(14)	0	0
OW9	0.5359(3)	0.91630(8)	0.5449(2)	0.0253(4)	0.0237(10)	0.0349(11)	0.0173(9)	-0.0010(7)	0.0028(8)	-0.0107(8)
OW10	0.9586(3)	0.99535(7)	0.7373(2)	0.0233(4)	0.0203(9)	0.0194(9)	0.0302(10)	0.0001(7)	-0.0064(8)	-0.0016(8)
OW11	0.5341(3)	0.25019(8)	0.7262(2)	0.0292(4)	0.0306(10)	0.0182(9)	0.0387(11)	0.0070(9)	-0.0124(9)	0.0004(9)
OW12	0.9644(3)	0.19572(7)	0.9484(2)	0.0238(4)	0.0273(10)	0.0267(10)	0.0174(9)	0.0022(7)	0.0000(8)	0.0048(8)
OW13	¾	0.15560(11)	0.7295(3)	0.0281(6)	0.0171(13)	0.0255(14)	0.0417(16)	-0.0129(12)	0	0
OW14	¾	0.29694(11)	0.9275(3)	0.0376(8)	0.0681(22)	0.0171(14)	0.0276(16)	-0.0019(12)	0	0
OW15	0.0114(3)	0.05941(8)	0.9812(2)	0.0329(5)	0.0421(13)	0.0272(11)	0.0293(11)	-0.0019(8)	0.0093(10)	-0.0003(9)
H11	0.834(4)	0.026(1)	0.487(3)							
H21	0.843(4)	0.880(1)	0.789(3)							
H31	0.453(5)	0.899(1)	0.573(3)							

H32	0.546(5)	0.909(1)	0.473(3)
H41	0.066(5)	0.976(1)	0.757(3)
H42	0.994(4)	0.025(1)	0.727(3)
H51	0.446(5)	0.228(1)	0.715(3)
H52	0.512(5)	0.277(1)	0.717(3)
H61	0.932(5)	0.182(1)	0.016(3)
H62	0.053(5)	0.174(1)	0.918(3)
H71	0.841(4)	0.136(1)	0.726(3)
H81	¾	0.317(2)	0.896(5)
H82	¾	0.300(2)	0.011(4)
H91	0.053(5)	0.081(1)	0.946(3)
H92	0.960(5)	0.076(1)	0.038(3)

Note: $A = 0.78(NH_4) + 0.22K$; The Uiso parameters for all H atoms were fixed at 0.04.

Table 4. Selected non-hydrogen bond distances (Å) in hazenite and its ammonium analogue

hazenite		NH_4-analogue of Hazenite	
K-O5	2.672(3)	A-O5	2.720(3)
-OW11 (x2)	2.980(2)	-OW11 (x2)	3.068(2)
-OW12 (x2)	2.908(2)	-OW12 (x2)	2.940(2)
-OW13	3.064(3)	-OW13	3.095(3)
Avg.	2.919	Avg.	2.972
Na-OW10 (x2)	2.563(3)	Na-OW10 (x2)	2.589(3)
-OW15 (x2)	2.425(3)	-OW15 (x2)	2.429(2)
-OW15 (x2)	2.472(3)	-OW15 (x2)	2.478(2)
Avg.	2.487	Avg.	2.498
Mg1-OW7	2.032(3)	Mg1-OW7	2.042(3)
-OW8	2.040(3)	-OW8	2.046(3)
-OW9 (x2)	2.066(2)	-OW9 (x2)	2.074(2)
-OW10 (x2)	2.083(2)	-OW10 (x2)	2.095(2)
Avg.	2.062	Avg.	2.071
Mg2-OW11 (x2)	2.060(2)	Mg2-OW11 (x2)	2.066(2)
-OW12 (x2)	2.074(2)	-OW12 (x2)	2.077(2)
-OW13	2.093(3)	-OW13	2.107(3)
-OW14	2.109(3)	-OW14	2.109(3)
Avg.	2.078	Avg.	2.084
P1-O1	1.544(3)	P1-O1	1.548(3)
-O2	1.540(3)	-O2	1.544(3)
-O3 (x2)	1.530(2)	-O3 (x2)	1.538(2)
Avg.	1.536	Avg.	1.542
P2-O4	1.535(3)	P2-O4	1.537(3)
-O5	1.534(3)	-O5	1.538(3)
-O6 (x2)	1.543(2)	-O6 (x2)	1.544(2)
Avg.	1.539	Avg.	1.541

Table 5. Comparison of unit-cell data for hazenite vs. NH_4-analogue of hazenite and struvite vs. struvite-K.

Name	Locality	*a* (Å)	*b* (Å)	*c* (Å)	*V* (Å^3)	References
Hazenite	Synthetic	6.9316(5)	25.1754(18)	11.2189(10)	1957.8(3)	Yang and Sun (2004)
Hazenite	Mono Lake	6.9349(4)	25.1737(15)	11.2195(8)	1958.7(2)	Yang et al. (2011)
NH_4-Hazenite	Run #1	6.962(1)	25.223(7)	11.293(2)	1983(1)	This study
NH_4-Hazenite	Run #2	6.9661(6)	25.236(3)	11.292(1)	1985.0(3)	This study
Struvite	Synthetic	6.955(1)	6.142(1)	11.218(2)	479.2(2)	Ferraris et al. (1986)
	Synthetic	6.966(1)	6.142(1)	11.217(2)	479.9(1)	Abbona et al. (1984)
Struvite	Run #1	6.956(2)	6.145(1)	11.226(4)	479.9(4)	This study
Struvite-K	Synthetic	6.873(2)	6.160(2)	11.087(3)	469.4(3)	Mathew (1979)
	Switzerland	6.892(2)	6.166(2)	11.139(4)	473.4(3)	Graeser et al. (2008)
Struvite-K	Run #9	6.8741(4)	6.1481(4)	11.1094(6)	469.51(4)	This study